

Integrable Atomtronic Interferometry

D. S. Grün¹, L. H. Ymai², K. Wittmann W.¹, A. P. Tonel², A. Foerster¹, and J. Links^{3,*}

¹*Instituto de Física da UFRGS, Avenida Bento Gonçalves, 9500 Porto Alegre, Rio Grande do Sul, Brazil*

²*Universidade Federal do Pampa, Avenida Maria Anunciação Gomes de Godoy, 1650 Bagé, Rio Grande do Sul, Brazil*

³*School of Mathematics and Physics, The University of Queensland, Brisbane 4072, Queensland, Australia*

 (Received 9 June 2020; accepted 23 May 2022; published 6 July 2022)

High sensitivity quantum interferometry requires more than just access to entangled states. It is achieved through the deep understanding of quantum correlations in a system. Integrable models offer the framework to develop this understanding. We communicate the design of interferometric protocols for an integrable model that describes the interaction of bosons in a four-site configuration. Analytic formulas for the quantum dynamics of certain observables are computed. These expose the system's functionality as both an interferometric identifier, and producer, of NOON states. Being equivalent to a controlled-phase gate acting on 2 hybrid qudits, this system also highlights an equivalence between Heisenberg-limited interferometry and quantum information. These results are expected to open new avenues for integrability-enhanced atomtronic technologies.

DOI: [10.1103/PhysRevLett.129.020401](https://doi.org/10.1103/PhysRevLett.129.020401)

Introduction.—Recent developments in the manipulation of wavelike properties in matter are driving a raft of atom-interferometric applications, in the vicinity of the Heisenberg limit, within the field of quantum metrology [1,2]. It has long been recognized that the ability to effectively and efficiently harness quantum interference is equivalent to implementing certain tasks in quantum computation [3]. Nowadays, ultracold quantum gases are proving to be successful in enabling quantum simulations for phenomena such as quantum magnetism and topological states of matter, beyond the capabilities of classical supercomputers [4]. Through a confluence of these types of investigations, there are several efforts to push research toward designs for atomtronic devices [5–7], based on circuits with atomic currents [8–11]. These devices promise high levels of control in the manipulation of many-body systems, leading to advanced sensitivity in metrology [12] and other quantum technologies [13–17].

Around a decade ago [18] a class of models was identified for physical realization of an interferometer, using dipolar atoms. The Hamiltonian governing the time evolution of the system is a generalized Bose-Hubbard model on four sites, with closed boundary conditions and long-ranged interactions. We begin by pinpointing a set of *integrable* couplings for the Hamiltonian, that is, choices of parameters for which there are four conserved operators, equal to the number of degrees of freedom. The property of integrability has two significant impacts: (i) integrable systems have unique properties, such as the Poisson distribution in energy level statistics [19], absence of chaotic behaviors [20], and nonstandard thermal equilibration [21]—the quantum Newton cradle [22] provided experimental verification of the latter—and

(ii) mathematically, integrability facilitates tractable, closed-form formulas to describe the physics.

In our study we utilize the conserved operators of the integrable system to guide the design of measurement protocols for interferometric tasks (see Fig. 1). Our results are applicable in a particular regime, designated as *resonant tunneling*, whereby the energy levels separate into distinct bands. Through an effective Hamiltonian approach, the entire energy spectrum and structure of eigenstates become explicit for resonant tunneling. Moreover, the system's behavior is clear in quantum information theoretic terms. The interferometer is equivalent to a system of two *hybrid qudits* [23], and the time evolution of states is equivalent to the operation of a *controlled-phase* gate [24,25]. We describe proof of principle examples of high-fidelity measurement protocols to identify and produce certain NOON states [1,3,26–28]. We also provide a

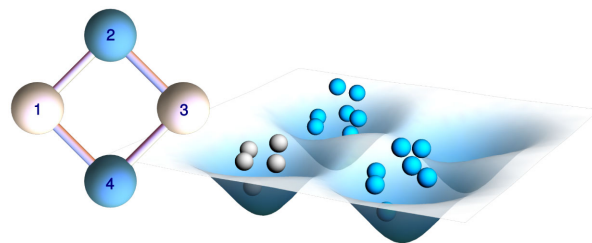


FIG. 1. Schematic representation of the interferometric circuit with tunneling between nearest neighbors. An initial state is prepared with M particles in site 1, and P particles in a (generally entangled) state across sites 2 and 4. After Hamiltonian time-evolution, measurement of particle number at site 3 is used to deduce information about the initial, or postmeasurement, state across sites 2 and 4.

physical-feasibility analysis of the system with first-principles calculations of the Hamiltonian parameters within an explicit Bose-atom setup (see the Supplemental Material, Sec. A [29]).

The model.—An extended Bose-Hubbard Hamiltonian on a square plaquette has the form [34,35]

$$H = \frac{U_0}{2} \sum_{i=1}^4 N_i(N_i - 1) + \sum_{i=1}^4 \sum_{j=1, j \neq i}^4 \frac{U_{ij}}{2} N_i N_j - \frac{J}{2} [(a_1^\dagger + a_3^\dagger)(a_2 + a_4) + (a_2^\dagger + a_4^\dagger)(a_1 + a_3)] \quad (1)$$

where $\{a_j, a_j^\dagger : j = 1, 2, 3, 4\}$ are canonical boson annihilation and creation operators, U_0 characterizes the short-range interactions between bosons at the same site, $U_{ij} = U_{ji}$ accounts for long-range (e.g., dipole-dipole) interactions between sites, and J represents the tunneling strength between neighboring sites. The Hamiltonian commutes with the total particle number $N = N_1 + N_2 + N_3 + N_4$ where $N_j = a_j^\dagger a_j$. Moreover, the Hamiltonian is integrable when $U_{13} = U_{24} = U_0$ and $U_{12} = U_{14} = U_{23} = U_{34}$. It acquires two additional conserved operators

$$Q_1 = \frac{1}{2} (N_1 + N_3 - a_1^\dagger a_3 - a_3^\dagger a_1),$$

$$Q_2 = \frac{1}{2} (N_2 + N_4 - a_2^\dagger a_4 - a_4^\dagger a_2),$$

such that $[Q_1, Q_2] = [Q_j, H] = [Q_j, N] = 0$, $j = 1, 2$. Integrability results from the derivation of the model through the quantum inverse scattering method. It is intimately related to exact solvability, due to the algebraic Bethe ansatz [36]. Hereafter we only consider the integrable case.

Resonant tunneling regime.—It is straightforward to check that there are large energy degeneracies when $J = 0$. From numerical diagonalization of Eq. (1), with N particles and a sufficiently small value of J , it is seen that the low-energy levels coalesce into well-defined bands [37], similar to that observed in an analogous integrable three-site model [14,38]. In this regime, an effective Hamiltonian H_{eff} is obtained through consideration of second-order tunneling processes. For an initial Fock state $|M - l, P - k, l, k\rangle$, with total boson number $N = M + P$, the effective Hamiltonian is a simple function of the conserved operators

$$H_{\text{eff}} = (N + 1)\Omega(Q_1 + Q_2) - 2\Omega Q_1 Q_2, \quad (2)$$

where $\Omega = J^2 / \{4U[(M - P)^2 - 1]\}$ with $U = (U_{12} - U_0)/4$. This result is valid for $J \ll U|M - P|$, which characterizes the resonant tunneling regime. For time evolution under H_{eff} , both $N_1 + N_3 = M$ and $N_2 + N_4 = P$ are constant. The respective $(M + 1)$ -dimensional subspace associated with sites 1 and 3 and $(P + 1)$ -dimensional subspace

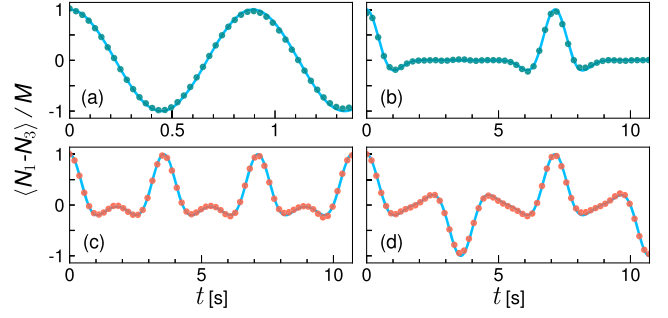


FIG. 2. Time evolution of expected fractional imbalance $\langle N_1 - N_3 \rangle / M$ (dot points) for the Hamiltonian [Eq. (1)] as a function of time t in units of seconds, with $U/J \simeq 1.2$, $U/\hbar \simeq 2\pi \times 19.5$ Hz, $J/\hbar \simeq 2\pi \times 16.2$ Hz, and different initial states: (a) $|4, 0, 0, 0\rangle$, (b) $|4, 11, 0, 0\rangle$, (c)–(d) $(|4, 11, 0, 0\rangle + \exp(i\phi)|4, 0, 0, 11\rangle)/\sqrt{2}$ with $\phi = 0$ (c) and $\phi = \pi$ (d). The top panels display agreement with the formula (3) (solid lines), while the bottom panels are in agreement with Eq. (5) (solid lines).

associated with sites 2 and 4 serve as 2 coupled, hybrid qudits [23], and provide the state space for the relevant energy band. This yields a robust approximation for the dynamics under Eq. (1), which we benchmark below. For later use we will designate the qudit associated with sites 1 and 3 as *qudit A*, and that associated with sites 2 and 4 as *qudit B*.

It is found through Bogoliubov transformations that the spectrum of H_{eff} is $E_{\text{eff}} = (N + 1)\Omega(q_1 + q_2) - 2\Omega q_1 q_2$ with $q_1 = 0, \dots, M$ and $q_2 = 0, \dots, P$. Thus the time evolution under H_{eff} is recognized as a controlled-phase gate [24,25]. From here, several analytic results are accessible. For the initial Fock state $|M, P, 0, 0\rangle$, the expectation value of the fractional imbalance $\mathcal{I}(t)$ between sites 1 and 3 is (in units where $\hbar = 1$)

$$\mathcal{I}(t) \equiv \langle N_1 - N_3 \rangle / M = \cos[(M + 1)\Omega t] [\cos(\Omega t)]^P. \quad (3)$$

When $P = 0$, there are harmonic oscillations in the imbalance. For nonzero P , the oscillations are no longer harmonic due to interference. For comparison, the results from numerical diagonalization of Eq. (1) are shown in the upper panels of Fig. 2.

Other initial states can be studied, such as

$$|\Phi(\phi)\rangle = \frac{1}{\sqrt{2}} |M, P, 0, 0\rangle + \frac{\exp(i\phi)}{\sqrt{2}} |M, 0, 0, P\rangle, \quad (4)$$

which is a product of a number state for site 1, vacuum for site 3 (qudit A), and a phase-dependent NOON state [1,3] across sites 2 and 4 (qudit B). We find the following result for the fractional imbalance between sites 1 and 3:

$$\begin{aligned} \langle N_1 - N_3 \rangle / M = & \cos[(M + 1)\Omega t] [\cos(\Omega t)]^P \\ & + \cos(\phi) \cos[(M + 1)\Omega t + \pi P/2] [\sin(\Omega t)]^P. \end{aligned} \quad (5)$$

This formula provides excellent agreement with numerical calculations using Eq. (1). Examples are provided, for choices $\phi = 0$ and $\phi = \pi$, in the lower panels of Fig. 2 using experimentally feasible parameters evaluated in the Supplemental Material, Sec. A [29].

NOON state identification and production.—The above results are sufficient to demonstrate the efficacy of the system to perform certain interferometric tasks. First consider a black box processor \mathbb{P} that outputs one of two possible NOON states, either symmetric or antisymmetric. The output state, with particle number P , is loaded into qudit B . With M particles in site 1 and zero in site 3 of qudit A , this composite initial state is given by Eq. (4) with either $\phi = 0$ (symmetric) or $\phi = \pi$ (antisymmetric). Choose M such that $N = M + P$ is odd, let the system evolve for time $t_m = \pi/(2\Omega)$, and then measure the particle number at site 3. According to Eq. (5), there are only two possible measurement outcomes. One is to obtain the outcome zero, which occurs with probability 1 when $\phi = \pi$. The other is to obtain the outcome M , which occurs with probability 1 when $\phi = 0$ (cf. the lower panels of Fig. 2, where the time of measurement is $t_m \simeq 3.57$ s). Moreover, this measurement is nondestructive, and the NOON state in qudit B is preserved [39].

This analytic result is an excellent approximation for the behavior governed by Eq. (1). From numerical results using the parameters of Fig. 2, we find that the success probability when $\phi = 0$ is 0.98334, and it is 0.99383 when $\phi = \pi$. This delivers a proof of principle example to show that the model (1) has the capacity to perform interferometry with high accuracy.

Remarkably, the earlier analysis on NOON state identification can now be inverted to show that the interferometer itself provides a high-fidelity simulation of the black box processor \mathbb{P} . For $|\Psi_0\rangle = |M, P, 0, 0\rangle$ with $N = M + P$ odd, it can be shown that

$$|\Psi(t_m)\rangle = \frac{(-1)^{(N+1)/2}}{2} |M, P, 0, 0\rangle + \frac{1}{2} |M, 0, 0, P\rangle + \frac{1}{2} |0, P, M, 0\rangle + \frac{(-1)^{(N-1)/2}}{2} |0, 0, M, P\rangle. \quad (6)$$

In accordance with the previous discussion, measurement at site 3 produces one of only two possible outcomes. A measurement outcome of M causes wave function collapse such that the state of qudit B is the symmetric (antisymmetric) NOON state if $(N + 1)/2$ is odd (even). Conversely, a measurement outcome of zero causes wave function collapse with an antisymmetric (symmetric) NOON state in qudit B if $(N + 1)/2$ is odd (even).

As before, it is useful to compare this result obtained from Eq. (2) against the analogous predictions of Eq. (1). Numerically, using the parameters of Fig. 2, we find that the outcome fidelity of this processor simulation for Eq. (1) is 0.97831 for outcome zero, and 0.99298 for outcome M ,

with respective probabilities of 0.49611 and 0.47639, close to the theoretically predicted values of 1/2 in each case. See the Supplemental Material, Sec. B [29], for further details, including probabilities and fidelities for intermediate outcomes.

Entanglement and correlations.—The ability to produce NOON states as described above is clearly dependent on the ability to create entanglement. More important is the ability to create “useful” entanglement since, as emphasized in the review article [1]: “Not all entangled states are useful for quantum metrology” (see also Ref. [46]). Below we demonstrate how this notion applies in the present context by analyzing the entanglement produced and the correlations present in the system.

It is convenient for our study to use the entanglement measure of *linear entropy* $\mathcal{E}(\rho)$, defined in terms of a density matrix $\rho(t) = |\Psi(t)\rangle\langle\Psi(t)|$ as [47,48] $\mathcal{E}(\rho) = 1 - \text{tr}(\rho^2)$. The linear entropy is bounded between 0 and $1 - 1/d$, where d is the dimension of the space on which the density matrix acts. For initial state $|\Psi_0\rangle = |M, P, 0, 0\rangle$ the entanglement between qudits A and B at time t_m is quantified through $\mathcal{E}[\rho_{1,3}(t_m)] = 1/2$, where $\rho_{1,3}(t_m) \equiv \text{tr}_{2,4}\rho(t_m)$ is the reduced density matrix (see the Supplemental Material, Sec. B [29], for details). This result is independent of P . It asserts that immediately prior to making a measurement at site 3, at time $t = t_m$, the entanglement between qudits A and B is *independent* of whether $N = M + P$ is even or odd.

Further, let $\rho_3(t_m) = \text{tr}_1[\rho_{1,3}(t_m)]$, which can be compactly expressed as

$$\rho_3(t_m) = \sum_{q=0}^M \mathcal{P}(q) |q\rangle\langle q|,$$

where $\mathcal{P}(q)$ refers to the probability of measuring q particles at site “3”. The linear entropy of ρ_3 quantifies the entanglement between the subsystems, sites 1 and 3, within qudit A . Now we encounter a significant difference between the even and odd cases. When N is odd, $\mathcal{E}[\rho_3(t_m)] = 1/2$. For even N , $\mathcal{E}[\rho_3(t_m)] = 1 - (1/2^{2M}) \binom{2M}{M} \sim 1 - (1/\sqrt{M\pi})$, where the second step invokes Stirling’s approximation. By symmetry, the same conclusion can be drawn for qudit B (with M replaced by P). The curious observation to make here is that in the odd case, which enables a protocol for NOON state production, the premeasurement entanglement *within* the qudits is substantially *less* than that for the even case. This is despite the premeasurement entanglement *between* the qudits being independent of number parity. While number-parity effects are ubiquitous in fermionic systems [49–53], they are less frequently encountered in bosonic models. The situation reported here displays some features in common with the work of Ref. [54].

A similar feature is observed in the correlations of the system. In order to quantify the effects of odd or even N , we

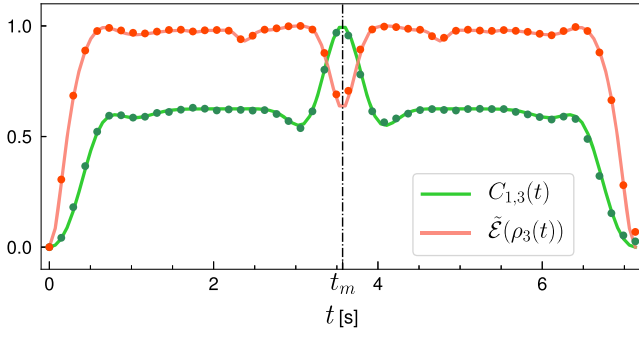


FIG. 3. Normalized linear entropy and NOON correlation function. The red (green) line depicts $\tilde{\mathcal{E}}[\rho_3(t)]$ [$C_{1,3}(t)$] calculated with the effective Hamiltonian H_{eff} of Eq. (2), while the dots illustrate the numerical values obtained with the Hamiltonian [Eq. (1)]. The initial state is $|\Psi_0\rangle = |4, 11, 0, 0\rangle$, and the Hamiltonian parameters are $U/\hbar = 2\pi \times 19.5$ Hz and $J/\hbar = 2\pi \times 16.2$ Hz.

first define the following NOON correlation function between sites “1” and “3”,

$$C_{1,3} = \frac{4}{M^2} (\langle N_1 \rangle \langle N_3 \rangle - \langle N_1 N_3 \rangle), \quad (7)$$

where $C_{1,3} = 1$ if there exists a NOON state at qudit A. Again for initial state $|\Psi_0\rangle = |M, P, 0, 0\rangle$, using Eq. (3) and the result $\langle (N_1 - N_3)^2 \rangle / M^2 = 1 + \alpha_M [\mathcal{I}(2t) - 1]$, $\alpha_M \equiv (M - 1)/(2M)$, yields

$$C_{1,3}(t) = 1 - \mathcal{I}^2(t) + \alpha_M [\mathcal{I}(2t) - 1]$$

and $C_{2,4}(t) = C_{1,3}(t)|_{M \leftrightarrow P}$ by symmetry. At $t = t_m$, we obtain $C_{1,3}(t_m) = M^{-1}$, $C_{2,4}(t_m) = P^{-1}$ for N even, and $C_{1,3}(t_m) = C_{2,4}(t_m) = 1$ for N odd where the last result asserts the simultaneous existence of NOON states in each of the qudits only for the odd case. The presence of a NOON state at $t = t_m$ is signaled by attaining the maximum of the NOON correlation function $C_{1,3}$ and a simultaneous dip in the normalized linear entropy $\tilde{\mathcal{E}}[\rho_3(t)] = (M + 1)\mathcal{E}[\rho_3(t)]/M$, as shown in Fig. 3. Further details on correlations between the qudits, and in particular the role of Eq. (5), are discussed in the Supplemental Material, Sec. C [29].

Heisenberg-limited interferometry.—Finally, we establish that the system is capable of interferometry with sensitivity at the Heisenberg limit, through the archetypal example of parameter estimation through the phase of a NOON state [1,3]. Consider initial state Eq. (4) with $N = M + P$ odd, and $\phi = 0$. A new phase φ is encoded into the bosons at site 4 through a transformation, $a_4^\dagger \mapsto \exp(i\varphi)a_4^\dagger$ (cf. Refs. [18,37]). This still corresponds to Eq. (4), but now with $\phi = P\varphi$, a phenomenon known as *phase super resolution* [27,28]. Again for time interval $t = t_m$, the imbalance between sites 1 and 3 is obtained from Eq. (5) as

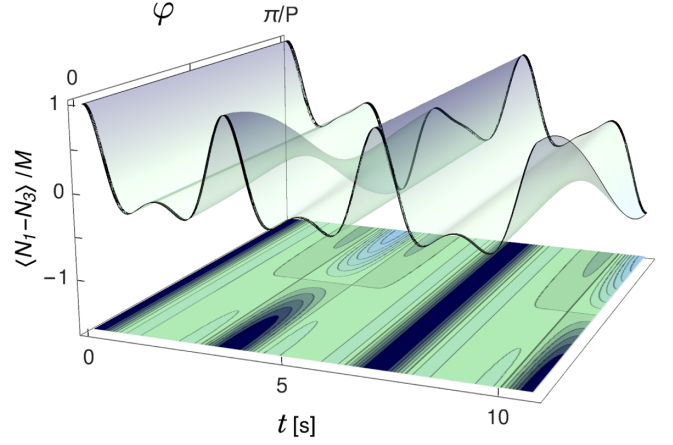


FIG. 4. Dependence of $\langle N_1 - N_3 \rangle / M$ as a function of time t (in units of seconds) and phase φ , for initial state [Eq. (4)] with $M = 4$, $P = 11$, $\phi = P\varphi$, and $U/J \simeq 1.2$. Upper surface: the colors range from light to dark blue, indicating lower and higher values for the imbalance fraction. The green color represents the region where $\langle N_1 \rangle \approx \langle N_3 \rangle$. Lower plane: the effect on the system’s dynamics is highlighted, specifically for the limiting cases $\varphi = 0$ and $\varphi = \pi/P$, where it is seen that there is a minimum-maximum inversion at $\varphi = \pi/(2P)$.

$$\langle N_1 - N_3 \rangle = (-1)^{(N+1)/2} M \cos(P\varphi) \quad (8)$$

providing the interference fringe with maximal contrast. Figure 4 shows the dependence of the fractional imbalance $\langle N_1 - N_3 \rangle / M$ on parameters φ and time t .

Next, it can be confirmed that $\langle (N_1 - N_3)^2 \rangle = M^2$, so

$$\begin{aligned} \Delta \langle N_1 - N_3 \rangle &= \sqrt{\langle (N_1 - N_3)^2 \rangle - \langle N_1 - N_3 \rangle^2} \\ &= M |\sin(P\varphi)|, \end{aligned}$$

where Δ denotes the standard deviation. Using the standard estimation theory approach [1,3], it is found that the system achieves Heisenberg-limited phase sensitivity since

$$\Delta\varphi = \frac{\Delta \langle N_1 - N_3 \rangle}{|d\langle N_1 - N_3 \rangle / d\varphi|} = \frac{1}{P}.$$

This is an improvement on the classical shot-noise case where $\Delta\varphi \sim 1/\sqrt{P}$ [1,3]. In the Supplemental Material, Sec. D [29], we present a discussion on the robustness of the system with respect to perturbation about the integrable case.

Conclusion.—We have provided an example of integrable atomtronic interferometry, through an extended Bose-Hubbard model, with four sites arranged in a closed square. The integrable properties of the model furnished the necessary tools to understand the dynamics of the system in the resonant tunneling regime. It allowed for the analytic calculation of dynamical expectation values and correlation functions heralding NOON state formation. This, in turn,

informed the relevant time interval required to implement certain measurement protocols. The probabilities for measurement outcomes [29] were computed via the density matrix. We demonstrated proof of principle examples that the integrable system functions as an identifier of NOON states produced by a black box processor, and as a simulator of such a processor.

Our study highlights the quantum information connections of the model by detailing its function as a hybrid qudit system subjected to a controlled-phase gate operation. This description complements other qudit studies in photonic [55–57] and NMR [58] settings, which are attracting attention due to the promise of increasing quantum computational capacity. It is anticipated that our results, in an atomtronic framework, may be transferable to these and other contexts. Besides providing feasibility for the physical setup and identifying means to experimentally probe the correlations between the qudits [29], the proposed scheme allows for further investigations of measurement-based protocols for novel quantum technologies. It also expands prospects for studying thermalization processes in the context of integrability.

In future research, we will undertake studies involving other states that may be useful for metrological applications, such as coherent states and Dicke states. We will examine the evolution of these input states, and investigate the correlations and the resulting generation of entanglement. Particular emphasis will be given to the understanding of multipartite entanglement generation, beyond the bipartite investigations reported here.

D. S. G. and K. W. W. were supported by CNPq (Conselho Nacional de Desenvolvimento Científico e Tecnológico), Brazil. A. F. acknowledges support from CNPq—Edital Universal 406563/2021-7. A. F. and J. L. received funding from the Australian Research Council through Discovery Project No. DP200101339. We thank Bing Yang and Ricardo R. B. Correia for very helpful discussions. J. L. acknowledges the traditional owners of the land on which The University of Queensland is situated, the Turrbal and Jagera people.

*Corresponding author.

jrl@maths.uq.edu.au

- [1] L. Pezzé, A. Smerzi, M. K. Oberthaler, R. Schmied, and P. Treutlein, *Rev. Mod. Phys.* **90**, 035005 (2018).
- [2] K. Bongs, M. Holynski, J. Vovrosh, P. Bouyer, G. Condon, E. Rasel, C. Schubert, W. P. Schleich, and A. Roura, *Nat. Rev. Phys.* **1**, 731 (2019).
- [3] H. Lee, P. Kok, and J. P. Dowling, *J. Mod. Opt.* **49**, 2325 (2002).
- [4] C. Gross and I. Bloch, *Science* **357**, 995 (2017).
- [5] R. A. Pepino, J. Cooper, D. Z. Anderson, and M. J. Holland, *Phys. Rev. Lett.* **103**, 140405 (2009).
- [6] R. Dumke *et al.*, *J. Opt.* **18**, 093001 (2016).

- [7] L. Amico, G. Birkel, M. Boshier, and L.-C. Kwek, *New J. Phys.* **19**, 020201 (2017).
- [8] A. Nunnenkamp, A. M. Rey, and K. Burnett, *Phys. Rev. A* **77**, 023622 (2008).
- [9] K. Stiebler, B. Gertjerenken, N. Teichmann, and C. Weiss, *J. Phys. B* **44**, 055301 (2011).
- [10] S. Ragole and J. M. Taylor, *Phys. Rev. Lett.* **117**, 203002 (2016).
- [11] T. Haug, R. Dumke, L.-C. Kwek, and L. Amico, *Commun. Phys.* **2**, 127 (2019).
- [12] S. Pandey, H. Mas, G. Drougakis, P. Thekkepatt, V. Bolpasi, G. Vasilakis, K. Poullos, and W. von Klitzing, *Nature (London)* **570**, 205 (2019).
- [13] M. K. Olsen and A. S. Bradley, *Phys. Rev. A* **91**, 043635 (2015).
- [14] K. W. Wilsmann, L. H. Ymai, A. P. Tonel, J. Links, and A. Foerster, *Commun. Phys.* **1**, 91 (2018).
- [15] T. Haug, J. Tan, M. Theng, R. Dumke, L. C. Kwek, and L. Amico, *Phys. Rev. A* **97**, 013633 (2018).
- [16] J. Polo, R. Dubessy, P. Pedri, H. Perrin, and A. Minguzzi, *Phys. Rev. Lett.* **123**, 195301 (2019).
- [17] E. Compagno, G. Quesnel, A. Minguzzi, L. Amico, and D. Feinberg, *Phys. Rev. Research* **2**, 043118 (2020).
- [18] T. Lahaye, T. Pfau, and L. Santos, *Phys. Rev. Lett.* **104**, 170404 (2010).
- [19] D. Poilblanc, T. Ziman, J. Bellissard, F. Mila, and G. Montambaux, *Europhys. Lett.* **22**, 537 (1993).
- [20] L. F. Santos and M. Rigol, *Phys. Rev. E* **81**, 036206 (2010).
- [21] P. Calabrese, F. H. L. Essler, and G. Mussardo, *J. Stat. Mech.* **06** (2016) 064001.
- [22] T. Kinoshita, T. Wenger, and D. S. Weiss, *Nature (London)* **440**, 900 (2006).
- [23] J. Daboul, X. Wang, and B. C. Sanders, *J. Phys. A* **36**, 2525 (2003).
- [24] A. Muthukrishnan and C. R. Stroud Jr., *Phys. Rev. A* **62**, 052309 (2000).
- [25] G. K. Brennen, D. P. O’Leary, and S. S. Bullock, *Phys. Rev. A* **71**, 052318 (2005).
- [26] G. J. Pryde and A. G. White, *Phys. Rev. A* **68**, 052315 (2003).
- [27] M. W. Mitchell, J. S. Lundeen, and A. M. Steinberg, *Nature (London)* **429**, 161 (2004).
- [28] K. J. Resch, K. L. Pregnell, R. Prevedel, A. Gilchrist, G. J. Pryde, J. L. O’Brien, and A. G. White, *Phys. Rev. Lett.* **98**, 223601 (2007).
- [29] See Supplemental Material at <http://link.aps.org/supplemental/10.1103/PhysRevLett.129.020401> for Sec. A, *Physical setup and parameter evaluations for the integrable system*; Sec. B, *Probabilities, fidelities and trade-off between fidelity and protocol time*, which includes Ref. [30]; Sec. C, *Correlations between qudits*, which includes Ref. [31]; and Sec. D, *Robustness of the interferometer*, which includes Refs. [32,33].
- [30] M. J. Gibbons, S. Y. Kim, K. M. Fortier, P. Ahmadi, and M. S. Chapman, *Phys. Rev. A* **78**, 043418 (2008).
- [31] R. Islam, R. Ma, P. M. Preiss, M. E. Tai, A. Lukin, M. Rispoli, and M. Greiner *Nature (London)* **528**, 77 (2015).
- [32] Y. Tang, W. Kao, K. Y. Li, S. Seo, K. Mallayya, M. Rigol, S. Gopalakrishnan, and B. L. Lev, *Phys. Rev. X* **8**, 021030 (2018).

- [33] C. Gross, T. Zibold, E. Nicklas, J. Estève, and M. K. Oberthaler *Nature (London)* **464**, 1165 (2010).
- [34] M. A. Baranov, *Phys. Rep.* **464**, 71 (2008).
- [35] T. Lahaye, C. Menotti, L. Santos, M. Lewenstein, and T. Pfau, *Rep. Prog. Phys.* **72**, 126401 (2009).
- [36] A. P. Tonel, L. H. Ymai, A. Foerster, and J. Links, *J. Phys. A* **48**, 494001 (2015).
- [37] D. S. Grün, W. K. Wittmann, L. H. Ymai, J. Links, and A. Foerster, *Commun. Phys.* **5**, 36 (2022).
- [38] A. P. Tonel *et al.*, *SciPost Phys. Core* **2**, 003 (2020).
- [39] Within the superlattice configuration [40] described in Supplemental Material A *Physical setup and parameter evaluations for the integrable system*, non-destructive measurement can be physically realized through Faraday imaging [41,42] or site-selective measurement [43,44] combined with off-resonant fluorescence imaging [45].
- [40] H.-N. Dai, B. Yang, A. Reingruber, H. Sun, X.-F. Xu, Y.-A. Chen, Z.-S. Yuan, and J.-W. Pan, *Nat. Phys.* **13**, 1195 (2017).
- [41] R. Yamamoto, J. Kobayashi, K. Kato, T. Kuno, Y. Sakura, and Y. Takahashi, *Phys. Rev. A* **96**, 033610 (2017).
- [42] D. Okuno, Y. Amano, K. Enomoto, N. Takei, and Y. Takahashi, *New J. Phys.* **22**, 013041 (2020).
- [43] B. Yang, H. N. Dai, H. Sun, A. Reingruber, Z. S. Yuan, and J. W. Pan, *Phys. Rev. A* **96**, 011602(R) (2017).
- [44] B. Yang *et al.*, *Science* **369**, 6503 (2020).
- [45] Y. H. Fung, A. Carpentier, P. Sompert, and M. Andersen, *Entropy* **16**, 582 (2014).
- [46] T. R. Bromley, I. A. Silva, C. O. Oncebay-Segura, D. O. Soares-Pinto, E. R. deAzevedo, T. Tufarelli, and G. Adesso, *Phys. Rev. A* **95**, 052313 (2017).
- [47] W. H. Zurek, S. Habib, and J. P. Paz, *Phys. Rev. Lett.* **70**, 1187 (1993).
- [48] F. Buscemi, P. Bordone, and A. Bertoni, *Phys. Rev. A* **75**, 032301 (2007).
- [49] K. A. Matveev and A. I. Larkin, *Phys. Rev. Lett.* **78**, 3749 (1997).
- [50] G. Zürn, A. N. Wenz, S. Murmann, A. Bergschneider, T. Lompe, and S. Jochim, *Phys. Rev. Lett.* **111**, 175302 (2013).
- [51] S. Matsuo, S. Nakaharai, K. Komatsu, K. Tsukagoshi, T. Moriyama, T. Ono, and K. Kobayashi, *Sci. Rep.* **5**, 11723 (2015).
- [52] C. Schilling and R. Schilling, *Phys. Rev. A* **93**, 021601(R) (2016).
- [53] E. T. Mannila, V. F. Maisi, H. Q. Nguyen, C. M. Marcus, and J. P. Pekola, *Phys. Rev. B* **100**, 020502(R) (2019).
- [54] D. Agboola, P. S. Isaac, and J. Links, *J. Phys. B* **51**, 145301 (2018).
- [55] R.-B. Jin, R. Shimizu, M. Fujiwara, M. Takeoka, R. Wakabayashi, T. Yamashita, S. Miki, H. Terai, T. Gerrits, and M. Sasaki, *Quantum Sci. Technol.* **1**, 015004 (2016).
- [56] M. Kues *et al.*, *Nature (London)* **546**, 622 (2017).
- [57] P. Imany, J. A. Jaramillo-Villegas, M. S. Alshaykh, J. M. Lukens, O. D. Odele, A. J. Moore, D. E. Leaird, M. Qi, and A. M. Weiner, *npj Quantum Inf.* **5**, 59 (2019).
- [58] A. Z. Khoury, A. M. Souza, L. E. Oxman, I. Roditi, R. S. Sarthour, and I. S. Oliveira, *Phys. Rev. A* **97**, 042343 (2018).